iScience

CellPress
OPEN ACCESS

Article

Cell-type specific circadian transcription factor BMAL1 roles in excitotoxic hippocampal lesions to enhance neurogenesis

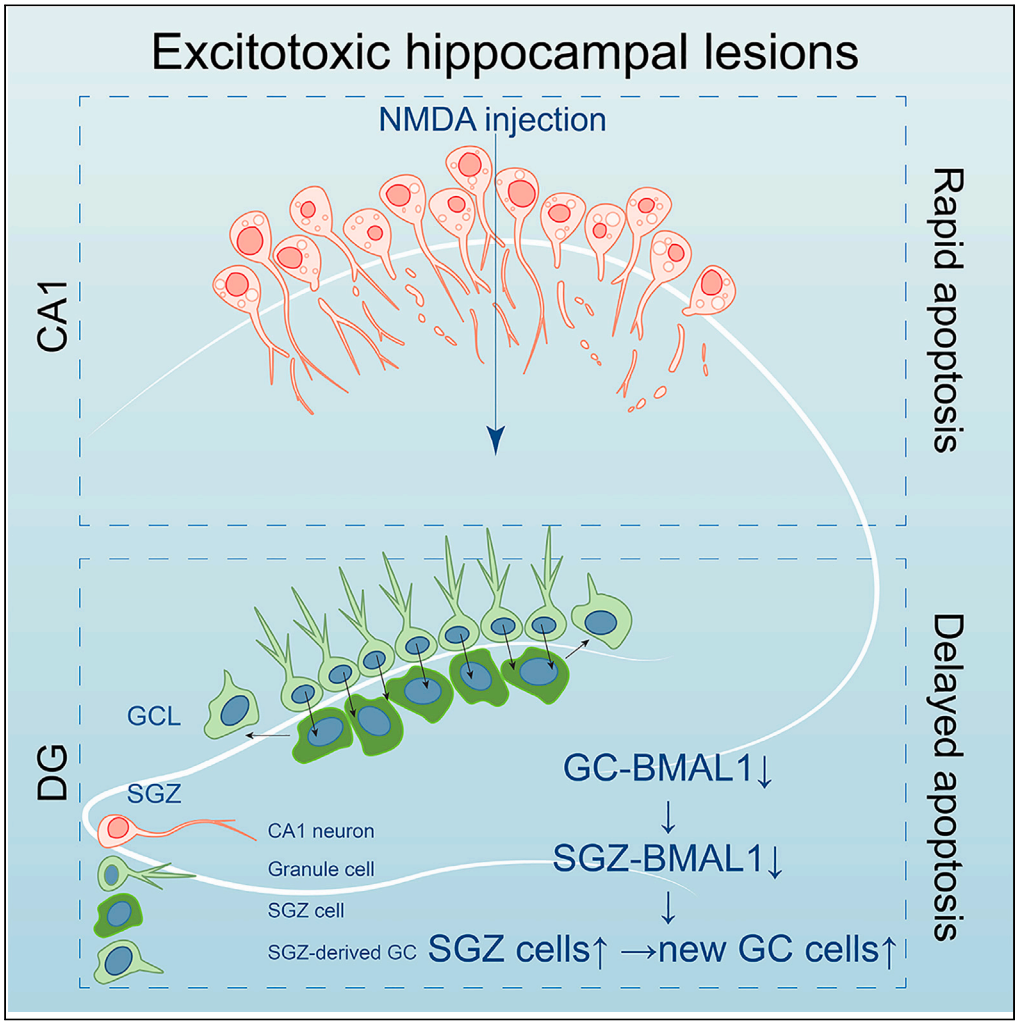

Xuebing Zhang, Suihong Huang, Jin Young Kim

jinykim@cityu.edu.hk

Highlights

Hippocampal neuronal BMAL1 responds to excitotoxicity to reduce its expression

Neural stem cell BMAL1 also responds to damaged neurons, reducing its expression

Altered BMAL1 enhances stem cell proliferation to replace damaged neurons

Zhang et al., iScience 27, 108829
February 16, 2024
https://doi.org/10.1016/j.isci.2024.108829

iScience

CellPress
OPEN ACCESS

Article

Cell-type specific circadian transcription factor BMAL1 roles in excitotoxic hippocampal lesions to enhance neurogenesis

Xuebing Zhang,[1] Suihong Huang,[2] and Jin Young Kim[1,3,*]

SUMMARY

Circadian clocks, generating daily rhythms in biological processes, maintain homeostasis in physiology, so clock alterations are considered detrimental. Studies in brain pathology support this by reporting abnormal circadian phenotypes in patients, but restoring the abnormalities by light therapy shows no dramatic effects. Recent studies on glial clocks report the complex effects of altered clocks by showing their beneficial effects on brain repairs. However, how neuronal clocks respond to brain pathology is elusive. This study shows that neuronal BMAL1, a core of circadian clocks, reduces its expression levels in neurodegenerative excitotoxicity. In the dentate gyrus of excitotoxic hippocampal lesions, reduced BMAL1 in granule cells precedes apoptosis. This subsequently reduces BMAL1 levels in neighbor neural stem cells and progenitors in the subgranular zone, enhancing proliferation. This shows the various BMAL1 roles depending on cell types, and its alterations can benefit brain repair. Thus, cell-type-specific BMAL1 targeting is necessary to treat brain pathology.

INTRODUCTION

Living organisms on Earth exhibit daily rhythms in various biological processes, from molecular to behavioral levels.[1,2] These rhythms are autonomously generated by endogenous oscillators called circadian clocks.[3] The core of circadian clocks is a conserved transcriptional-translational negative feedback loop that is operated by the transcription factor BMAL1/CLOCK heterodimer and its inhibitors *Period* (*Per*) and *Cryptochrome* (*Cry*).[4,5] BMAL1/CLOCK binds to E-box sites on promoters to transcribe thousands of its target genes (clock genes), including *Per* and *Cry* genes.[6] PERs and CRYs form large nuclear complexes with transcriptional corepressors (PER complexes), bringing them to BMAL1/CLOCK to inhibit its activity.[7] Degradation of PERs and CRYs releases BMAL1/CLOCK from PER complexes to start a new cycle.[8] Thus, biological processes operated by clock gene products show rhythmicity with a 24-h cycle in their activities, thereby maintaining homeostasis. Clock genes also include a transcription factor retinoic acid-related orphan receptor α (*Rorα*) and its inhibitors REV-ERBα/β (*Nr1d1/2*) that build an additional loop coupled to the negative feedback loop through *Bmal1* expression.[5]

Circadian clocks are intrinsic to most cells, including neural cells.[9] Individual clocks in the body synchronize together using signals from local environments. Light information captured by retinal photoreceptors is the strongest signal to synchronize all clocks in the body.[10] Ganglion cells receive photic information and convey it to the circadian pacemaker suprachiasmatic nucleus (SCN) in the hypothalamus by releasing neurotransmitter glutamate and neuromodulator pituitary adenylyl cyclase-activating peptide (PACAP).[11–13] Glutamate acts at N-methyl-D-aspartate (NMDA) receptors on SCN neurons and phosphorylates a transcription factor cAMP-responsive element-binding protein (CREB).[14,15] Phosphorylated CREB (pCREB) transcribes *Per1* and *Per2* in BMAL1-independent ways, but PER1 and PER2 expressed by pCREB can repress BMAL1/CLOCK to incorporate photic information into SCN clocks.[16,17] Similarly, SCN neurons projecting to other brain areas directly or indirectly communicate with neural cells via neurocircuits and humoral cues.[18,19] The signals generated by SCN clocks change microenvironments in target areas, and non-SCN clocks respond to these to be synchronized.[20] Through clock-clock communications in different areas and cells, circadian clocks, including BMAL1 activities, can be synchronized together and orchestrate physiological processes.

Accumulated studies have reported altered circadian phenotypes in patients with neurodegenerative diseases, from molecular to behavioral levels.[21] For example, abnormal circadian patterns in clock gene expression, hormone production and secretion, and sleep were observed in patients with Alzheimer's and Parkinson's disease.[22–24] Although underlying molecular mechanisms are elusive, clinical trials have tried resetting patients' abnormal circadian phenotypes with light therapy and melatonin administration.[21,25–27] Since circadian rhythmic activities of physiological processes maintain homeostasis, resetting abnormal circadian phenotypes in patients was believed to restore homeostasis, thereby helping treatments. However, many clinical trials ended with no significant effects on delaying disease progression or improving symptoms.[21] This hints that altered circadian phenotypes result from multiple underlying mechanisms, and some may be related

[1]Department of Biomedical Sciences, City University of Hong Kong, Hong Kong SAR, China
[2]Jockey Club College of Veterinary Medicine and Life Sciences, City University of Hong Kong, Hong Kong SAR, China
[3]Lead contact
*Correspondence: jinykim@cityu.edu.hk
https://doi.org/10.1016/j.isci.2024.108829

to other processes like repair. Recent studies about glial clocks support this idea—altered glial clocks help brain repair. Reduced astrocytic BMAL1 activities in demyelinating lesions enhanced remyelination by recruiting adult neural stem cells (NSCs) to the lesions.[28] Deletion of glial *Bmal1* was involved in amyloid-β clearance by increasing glial phagocytic activities in the brain of an Alzheimer's animal model.[29] Reduced BMAL1 in microglia suppressed pro-inflammatory activities but induced anti-inflammatory activities via altered clock gene expression.[30] However, to our knowledge, almost no studies elucidate how neuronal clocks respond to pathological conditions and their consequences.

RESULTS

NMDA-induced excitotoxicity mimics neurodegenerative conditions in the adult hippocampus

To study neuronal clock functions, we chose glutamate excitotoxicity as an experimental model because excitotoxicity is frequently detected in various brain pathologies.[31] To mimic excitotoxicity in the adult mouse brain, we employed stereotaxic injection to locally inject the glutamate agonist NMDA into the hippocampus of Thy1-YFP-16 transgenic mice expressing yellow fluorescent protein (YFP) in neurons. NMDA (excitotoxicity) or phosphate buffer saline (PBS; control) was injected into either side of the brain. On day 1 (Excito-1D) and day 3 (Excito-3D), the brains were harvested and processed to monitor the states of YFP^+ neurons. In Excito-1D, significantly fewer and damaged YFP^+ neurons were observed in the hippocampal cornu ammonis 1 (CA1) and dentate gyrus (DG) areas than in the control side (white arrows in Figures 1A–1C). In CA1 neurons, significant axonal damages were also observed (Figures 1B and 1C). In Excito-3D, almost no YFP^+ neurons were detected in the CA1 and DG (Figures 1A–1D). This shows that NMDA damages neurons in the hippocampus to mimic glutamate excitotoxicity.

In the same experimental condition, RNAs were extracted from the hippocampi to examine the expression patterns of neural cell markers—*Thy1* and *Map2* for neurons; *Mbp* for oligodendrocytes; *Gfap* and *Itgam* for reactive astrocytes and activated microglia, respectively. The expression of neuronal markers *Thy1* and *Map2* was gradually and significantly reduced in Excito-1D and 3D compared to the control. However, *Mbp*, *Gfap*, and *Itgam* expression were significantly increased in excitotoxic lesions. A control gene, *Rpl30*, showed similar expression levels in all conditions (Figure S1A). This shows that excitotoxicity damages and reduces neurons, not oligodendrocytes, astrocytes, and microglia. In addition, induced *Gfap* and *Itgam* expression indicates reactive astrocytes and activated microglia in excitotoxic lesions, which are well-known features of glutamate excitotoxicity.[32,33] This confirms reduced neurons in excitotoxic hippocampal lesions but not other neural cell types.

Since reduced YFP^+ neurons were observed in the CA1 and DG of Excito-1D and 3D, we hypothesized that excitotoxicity induces neuronal damage and apoptosis in both areas. To test this, we first measured the expression of damaged neuron (*cFos*) and apoptosis (*Caspase3*) markers in excitotoxic hippocampal lesions. Compared to the control, induced *cFos* and *Caspase3* expression in Excito-1D and 3D confirmed neuronal damage and apoptosis by excitotoxicity (Figure S1B). Next, we performed TUNEL assays in brain sections to detect DNA fragmentation (a maker of the last stage of apoptosis) in excitotoxic hippocampal lesions. As expected, TUNEL signals appeared in the CA1 of Excito-1D (Figures 1E, 1F, and S1C), and more $TUNEL^+$ nuclei were detected in Excito-3D (white arrowheads in Figure 1E). This shows that excitotoxicity rapidly induces the apoptosis process in the CA1, consistent with significantly reduced YFP^+ neurons in the CA1 of Excito-1D. However, interestingly, we observed almost no detectable TUNEL signals in the DG of Excito-1D and 3D (red arrows in Figures 1E and S1C). $TUNEL^+$ cells were later detected in excitotoxic DG lesions like Excito-7D (data not shown). This suggests that excitotoxicity differentially induces the apoptosis process in the CA1 and DG, rapidly in the CA1 but delayed in the DG.

Excitotoxicity reduces BMAL1 levels in hippocampal neurons

In the SCN, glutamate-activated NMDA receptors (NMDARs) phosphorylate CREB to inhibit BMAL1 activity via its inhibitor *Per1* and *Per2* expression.[16,17] This hinted that over-activated NMDARs by excitotoxicity might affect circadian clocks in the hippocampus. To study this, we first confirmed the circadian rhythmic expression of core clock genes in the hippocampus to gain insight into hippocampal clocks. The hippocampi were harvested from wild-type mice every 4 h across a day, followed by RNA extractions and qRT-PCR to examine clock gene expression patterns. R package MetaCycle was used to evaluate the rhythmicity in time-series data. The analysis results confirmed all clock gene expression (*Bmal1*, *Per1*, *Per2*, *Cry1*, and *Nr1d2*) in the hippocampus as rhythmic (Figure S2A). The *Bmal1* expression peaked at circadian time (CT)06, and its target gene *Per1*, *Per2*, *Cry1*, and *Nr1d2* expression peaked at CT14 and CT18 (Figures S2A and S2B). Since BMAL1 is the circadian transcription factor, its changes significantly affect other clock gene expression, followed by altered molecular clock activities and circadian rhythms. Thus, we decided to study neuronal BMAL1 responses in excitotoxic hippocampal lesions at CT06 when its expression peaks in the hippocampus.

Activated NMDARs affect SCN-neuronal BMAL1 via pCREB-dependent BMAL1 inhibitor expression.[16,17] To examine whether excitotoxicity affects neuronal BMAL1 via a pCREB-dependent mechanism, we examined pCREB levels. After BMAL1 antibody validation (Figure S3A), coronal brain sections of control and excitotoxic mice were processed for immunostaining with anti-pCREB and BMAL1 antibodies. In control mice, almost no pCREB signals ($pCREB^-$) were detected in both CA1 and DG areas. In Excito-1D, increasing $pCREB^+$ cells were detected in the CA1 (Figures 2A and 2B). As expected, $pCREB^+$ cells exhibited low BMAL1 levels ($BMAL1^-$, red arrowheads in Excito-1D of Figure 2A), and BMAL1-expressing cells showed low pCREB signals (white arrowheads in Excito-1D of Figure 2A). In Excito-3D, most CA1 cells showed high pCREB signals with low BMAL1 levels (Figures 2A and 2B). Interestingly, excitotoxic DG lesions showed different patterns from CA1 lesions. Most DG cells in Excito-1D and 3D showed reduced BMAL1 levels than the control, similar to CA1 lesions (Figures 2A–2C). However, pCREB signals were not detectable in most $BMAL1^-$ DG cells (the middle graph in Figure 2C). In addition, a few cells in the DG of Excito-3D expressed BMAL1 (white arrowheads in Excito-3D of Figure 2A). Except for CA1 and DG areas, BMAL1 levels in the NMDA-injection site, between the

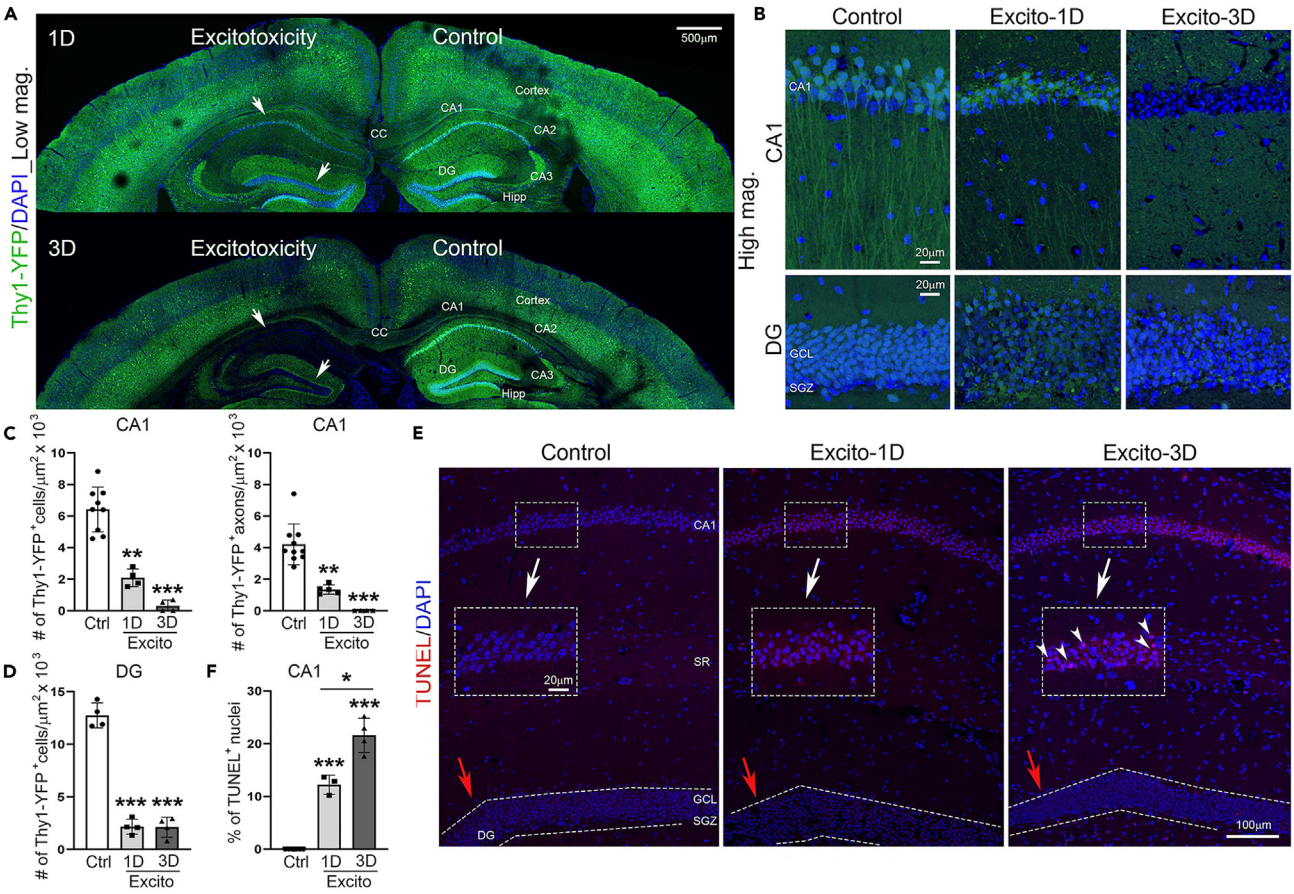

Figure 1. NMDA-induced excitotoxicity mimics neurodegenerative conditions in the adult hippocampus

(A) Confocal images of Thy1-YFP transgenic mouse brains in control and excitotoxicity on day 1 (Excito-1D) and day 3 (Excito-3D). Tiled overview scans of the brains (Low mag.). PBS and NMDA were stereotaxically injected into either side of the hippocampus as control and excitotoxicity. White arrows indicate reduced YFP^+ neurons in the CA1 and DG of excitotoxicity. DAPI (blue) was used as a nuclear counterstain.

(B) Cropped and amplified images of (A) in high magnification (High mag.).

(C) The quantification of CA1 areas in (B) (mean ± SD; a dot indicates one mouse brain; two-tailed t-test). Control (Ctrl) and excitotoxicity (Excito) on day 1 (1D) and day 3 (3D).

(D) The quantification of DG areas in (B) (mean ± SD; a dot indicates one mouse brain; two-tailed t-test).

(E) Confocal micrographs of control and excitotoxic hippocampal lesions, stained with TUNEL (red). DAPI (blue) was used as a nuclear counterstain. White arrows indicate amplified images of CA1 areas in the dashed rectangles. White dashed lines and red arrows indicate the DG. Images from maximum intensity projections.

(F) The quantification of CA1 areas in (E) (mean ± SD; a dot indicates one mouse brain; two-tailed t-test).

*p < 0.01; **p < 0.001; ***p < 0.0001. See also Figures S1.

CA1 and DG (the stratum radiatum, stratum lacunosum-moleculare, and molecular DG layer), showed no significant differences between control and excitotoxicity (Figure S3B). Also, no cell was positive for both BMAL1 and pCREB in all conditions. This shows excitotoxicity reduces BMAL1 levels in the CA1 and DG via pCREB-dependent and -independent mechanisms, respectively.

Granule cells with reduced BMAL1 in excitotoxic DG lesions subsequently reduce SGZ BMAL1 to induce SGZ cell proliferation

We next asked for reduced BMAL1 roles in excitotoxic hippocampal lesions. Figure 1 shows rapidly induced apoptosis in the CA1 in response to excitotoxicity—decreased YFP^+ cells and increased TUNEL signals in Exicto-1D. In the DG lesions, although YFP^+ cell numbers were decreased, $TUNEL^+$ cells were not yet detected in Excito-1D and 3D. Based on this, we decided to focus on excitotoxic DG lesions to study reduced BMAL1 roles because delayed apoptosis distinguishes reduced BMAL1 effects from apoptosis effects, which are simultaneously observed in the CA1 of Exicto-1D.

To understand the roles of reduced BMAL1, we further investigated excitotoxic DG lesions. The DG is divided into two parts: the granule cell layer (GCL) with granule cells/neurons (GCs) and the subgranular zone (SGZ) with adult NSCs and transiently amplifying intermediate

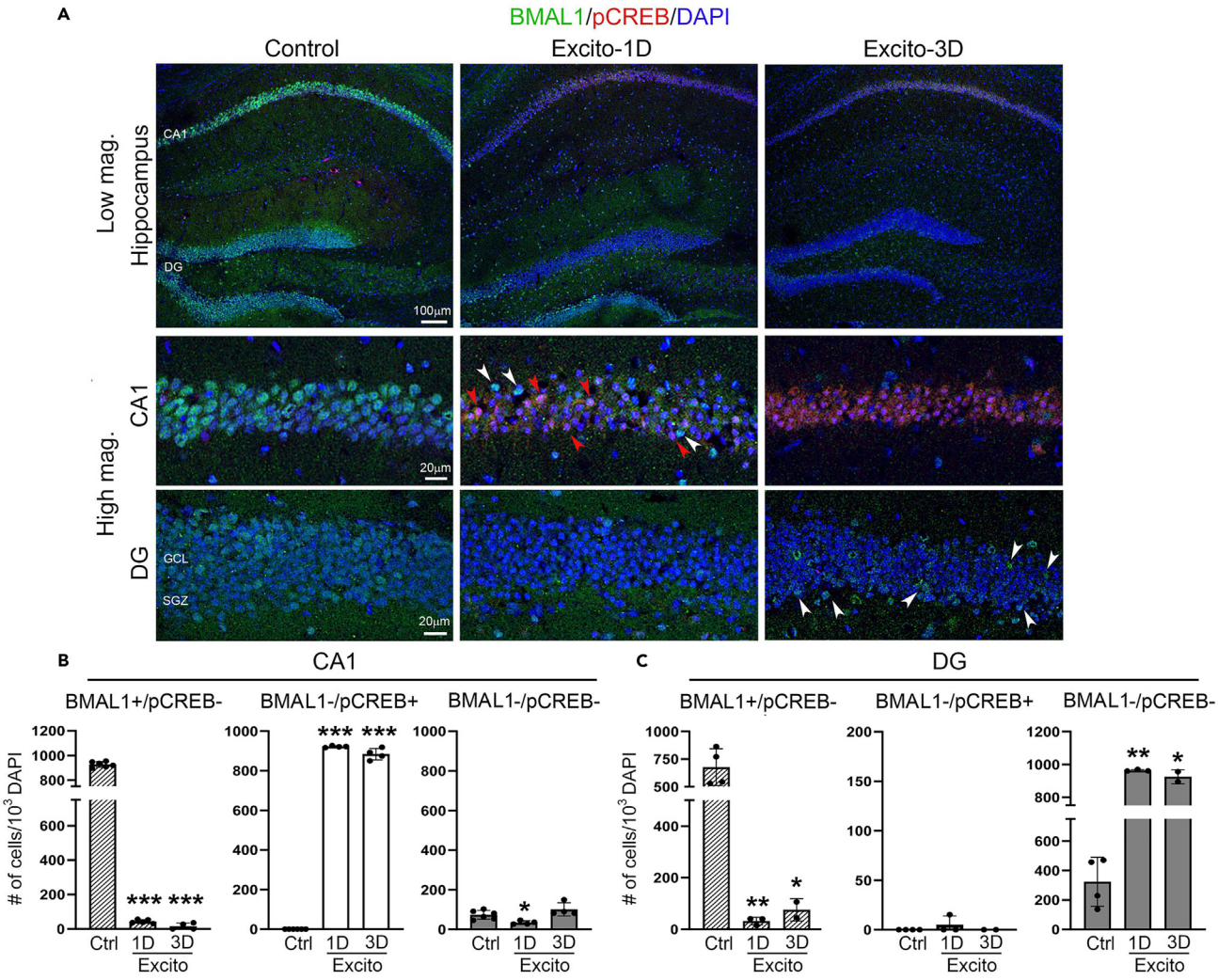

Figure 2. Excitotoxicity reduces BMAL1 levels in hippocampal neurons

(A) Confocal images of control and excitotoxic hippocampal lesions, stained with antibodies against BMAL1 (green) and pCREB (red). DAPI (blue) was used as a nuclear counterstain. White and red arrowheads indicate BMAL1^{+}/pCREB^{-} and BMAL1^{-}/pCREB^{+} cells, respectively.

(B) The quantification of CA1 areas in (A) (mean ± SD; a dot indicates one mouse brain; two-tailed t-test). Control (Ctrl) and excitotoxicity (Excito) on day 1 (1D) and day 3 (3D).

(C) The quantification of DG areas in (A) (mean ± SD; a dot indicates one mouse brain; two-tailed t-test).

*p < 0.01; **p < 0.001; ***p < 0.0001. See also Figures S2 and S3.

progenitors (SGZ cells).[34] In physiological conditions, GCs project to the CA3 areas to communicate via neural circuits. In pathological conditions, SGZ cells respond to damaged GCs to replace them. It is well-known that circadian clocks in SCN neurons projecting to other brain regions communicate with clocks in target areas via neural circuits and secreted cues to synchronize local clocks.[11,12] So, we asked whether reduced BMAL1 in excitotoxic DG lesions affects BMAL1 in GC projecting CA3 neurons or neighbor SGZ cells (Figure 3A). We first examined whether BMAL1 in CA3 cells was affected by excitotoxic DG lesions by immunostaining. In our excitotoxicity model, local NMDA injection reduced YFP signals mainly in the CA1 and DG but not in the CA3 (Figure 1A). In Excito-1D and 3D, reduced GC-BMAL1 did not affect CA3-BMAL1 levels (Figures 3B and 3C). This means excitotoxicity directly reduces BMAL1 levels in GCs, but GC-BMAL1 does not convey this information into the projecting area via neural circuits.

We next examined the effects of GC-BMAL1 in excitotoxic DG lesions on neighbor SGZ cells. In the SGZ, NSCs with a radial process that traverses the GCL give rise to intermediate progenitors with rounded morphology. Then, intermediate progenitors generate migratory immature granule cells with neurite morphology.[35–37] Since SGZ cells maintain stemness in physiological conditions, most express lower NMDAR levels, thereby minor NMDA direct effects on SGZ cells.[38] We first confirmed whether NMDA directly affects SGZ-BMAL1. Primary mature neurons and SGZ cells were cultured, and then relative mRNA levels of NMDAR subunits (NMDAR2A and NMDAR2B) were compared. Compared to mature neurons, NDMAR subunit expression levels were minor in SGZ cells (Figure S4A). Next, cultured SGZ cells were treated

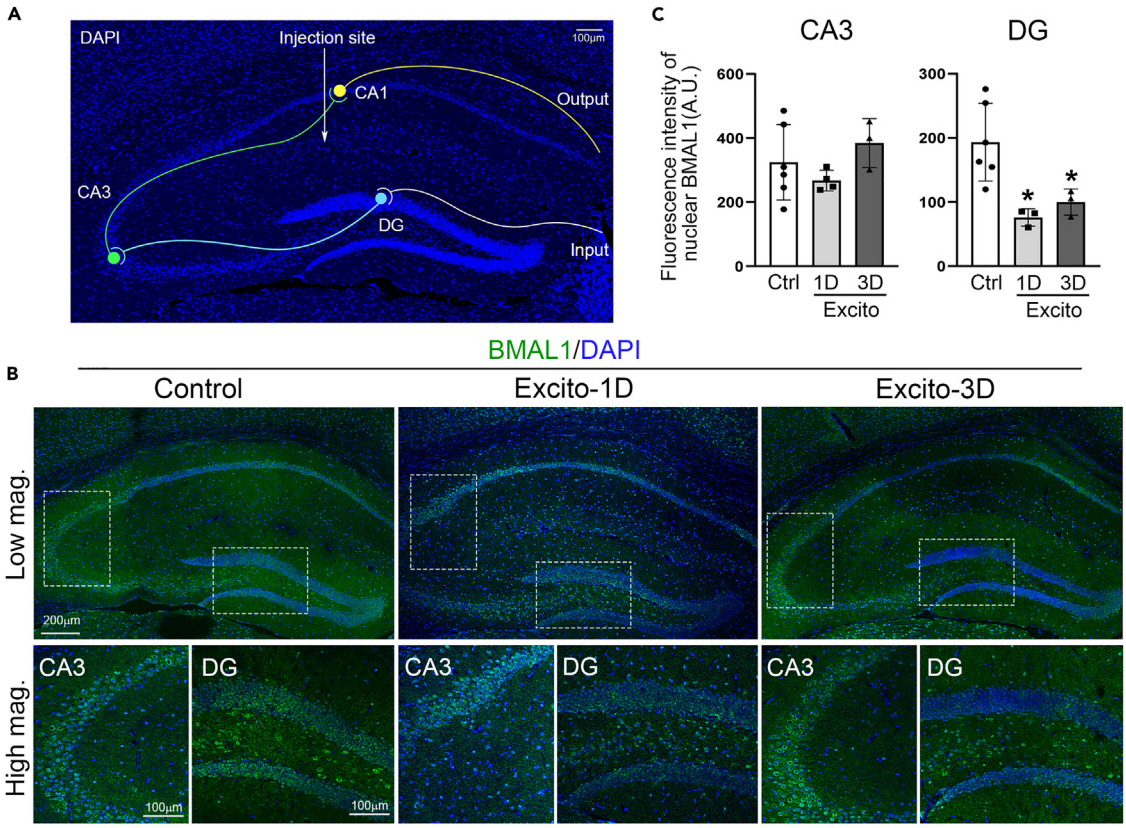

Figure 3. Reduced BMAL1 in excitotoxic DG lesions does not affect BMAL1 levels in the CA3

(A) Simplified schematic neuronal projections in the hippocampus. White arrow indicates PBS or NMDA injection site.

(B) Confocal images of control (PBS injection) and excitotoxic hippocampal lesions on day 1 (Excito-1D) and day 3 (Excito-3D), stained with anti-BMAL1(green) antibodies. Tiled overview scans of the hippocampi. The dashed rectangles in the lower magnification images (Low mag.) indicate amplified areas in the high magnification images (High mag.). CA3 and DG areas are amplified in the lower images. DAPI (blue) was used as a nuclear counterstain.

(C) The quantification of nuclear BMAL1 fluorescence intensity in CA3 and DG areas in (B) (mean ± SD; a dot indicates one mouse brain; two-tailed t-test). *$p < 0.05$.

with either NMDA or vehicle to examine whether NMDA directly affects SGZ-BMAL1 and apoptosis. No differences were detected in *Bmal1* and *Caspase 3* levels in NMDA-treated SGZ cells compared to the control (Figure S4B). This means that NMDA has no significant direct effect on SGZ-BMAL1 and does not induce SGZ apoptosis. Therefore, if SGZ cells are altered in excitotoxic DG lesions, signals are from damaged GCs rather than NMDA.

To examine how SGZ cells respond to excitotoxic DG lesions, we induced excitotoxicity in Nestin-EGFP transgenic mice expressing enhanced green fluorescent protein (EGFP) in NSCs and progenitors. After NMDA injections, the brains were harvested from Excito-1D and 3D mice and processed for immunostaining with anti-BMAL1 antibodies to monitor $EGFP^+$-SGZ cell behavior and its BMAL1 levels. BMAL1-expressing GCs and $EGFP^+$ cells were observed in the GCL and SGZ of control mice in Figure 4A. In Excito-1D and 3D, we observed gradually increasing $EGFP^+$ cells in the SGZ (Figures 4A and 4B). In Excito-3D, a few $EGFP^+$ cells migrated from the SGZ to the GCL, and significant numbers of $EGFP^+$ cells showed neurite morphology compared to $EGFP^+$ cells in control (Figures 4A and 4C). Note that a feature of immature GCs is neurite morphology.[35,36] This shows that excitotoxicity in the DG induces SGZ cell numbers and drives their migration and differentiation.

We next examined BMAL1 in $EGFP^+$ cells in excitotoxic DG lesions. In control, the majority of $EGFP^+$ cells expressed BMAL1 (Figures 4A and 4D). In Excito-1D, compared to the control, the increased number of $EGFP^+$ cells exhibited almost no detectable BMAL1 ($BMAL1^-$/$EGFP^+$), and $BMAL1^+$/$EGFP^+$ cell number was decreased (Figure 4D). In Excito-3D, we observed similar patterns with Excito-1D in $EGFP^+$ cells—increased numbers of total $EGFP^+$ and $BMAL1^-$/$EGFP^+$ cells compared to the control. However, when we compared Excito-1D and 3D, we found more $BMAL1^+$/$EGFP^+$ cells in Excito-3D than in Excito-1D (red arrowheads in Figures 4A and 4D). This suggests that reduced SGZ-BMAL1 in excitotoxic DG lesions switches NSCs to transiently amplifying intermediate progenitors to increase cell numbers. Once progenitors start differentiation into migratory immature granule cells (determining cell fate), they re-express BMAL1 to become BMAL1-expressing mature GCs.

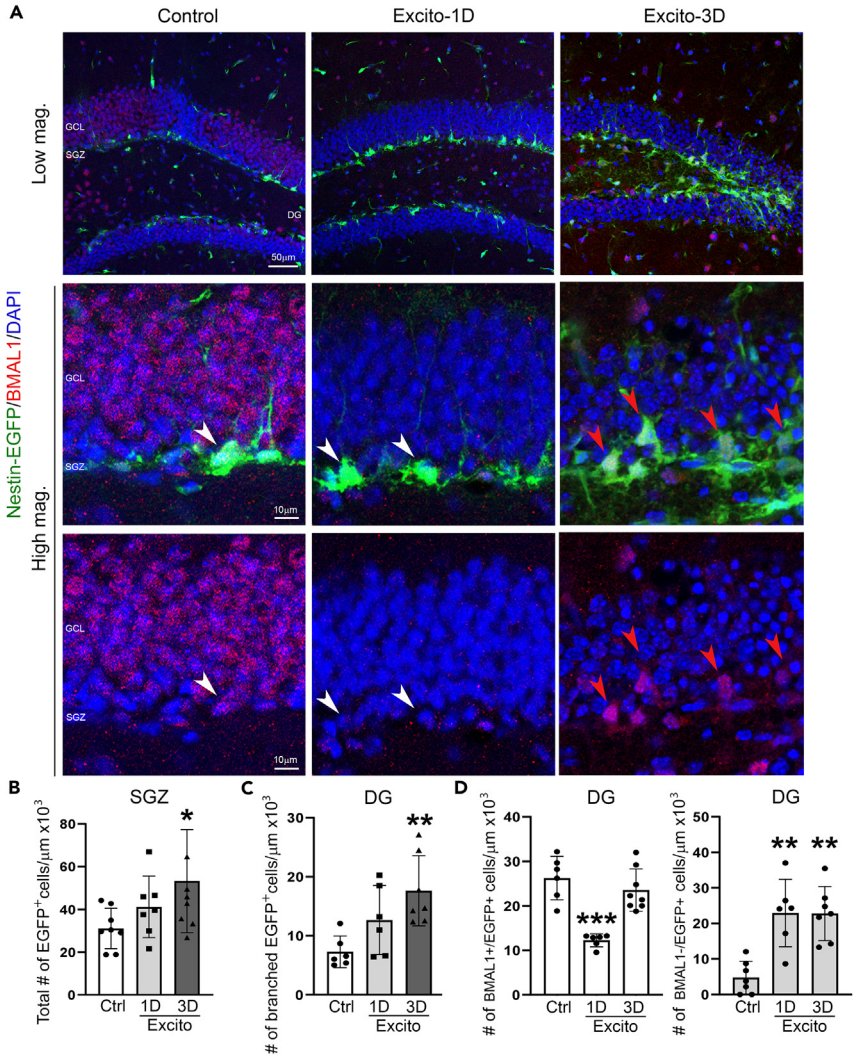

Figure 4. Granule cells with reduced BMAL1 in excitotoxic DG lesions subsequently reduce SGZ BMAL1 to induce SGZ cell proliferation

(A) Confocal micrographs of Nestin-EGFP transgenic mice in control and excitotoxicity on day 1 (Excito-1D) and day 3 (Excito-3D), stained with anti-BMAL1 (red) antibodies. Overview scans of the DG in low magnification (Low mag.) and cropped and amplified images in high magnification (High mag.). The white arrowhead in the control indicates BMAL1$^+$/EGFP$^+$ cells. White arrowheads in Excito-1D indicate BMAL1$^-$/EGFP$^+$ cells. Red arrowheads in Excito-3D indicate BMAL1$^+$/EGFP$^+$ cells. DAPI (blue) was used as a nuclear counterstain.

(B) The quantification of the SGZ in (A) (mean ± SD; a dot indicates one mouse brain; two-tailed t-test). Control (Ctrl) and excitotoxicity (Excito) on day 1 (1D) and day 3 (3D).

(C) The quantification of the DG in (A) (mean ± SD; a dot indicates one mouse brain; two-tailed t-test).

(D) The quantification of the DG in (A) (mean ± SD; a dot indicates one mouse brain; two-tailed t-test).

*p < 0.05; **p < 0.01; ***p < 0.0001. See also Figures S4.

Since EGFP$^+$ cell numbers were increased in excitotoxic DG lesions compared to the control, we examined cell proliferation in Excito-1D and 3D. For this, RNAs extracted in the hippocampi of control and excitotoxic mice were processed to measure *Ki67*, *p27*, *Sox2*, and *Pdgfrα* expression levels. Induced cell proliferation marker *Ki67* and reduced cell cycle inhibitor *p27* expression were observed in Excito-1D and 3D compared to the control, meaning increased cell proliferation. Then, the expression of stem cell marker *Sox2* and oligodendrocyte progenitor (OPC) maker *Pdgfrα* were examined. Significantly increasing *Sox2* levels and no changed *Pdgfrα* expression suggest increased EGFP$^+$ cells in excitotoxic DG lesions are from stem cell proliferation than OPC proliferation (Figure S4C). We also confirmed that NMDA did not induce SGZ cell proliferation directly by detecting no significant changes in *Ki67* and *p27* expression in NMDA-treated SGZ cells (Figure S4B). This suggests that damaged GCs in excitotoxic DG lesions induce the proliferation of NSCs and neuronal progenitors rather than local OPCs.

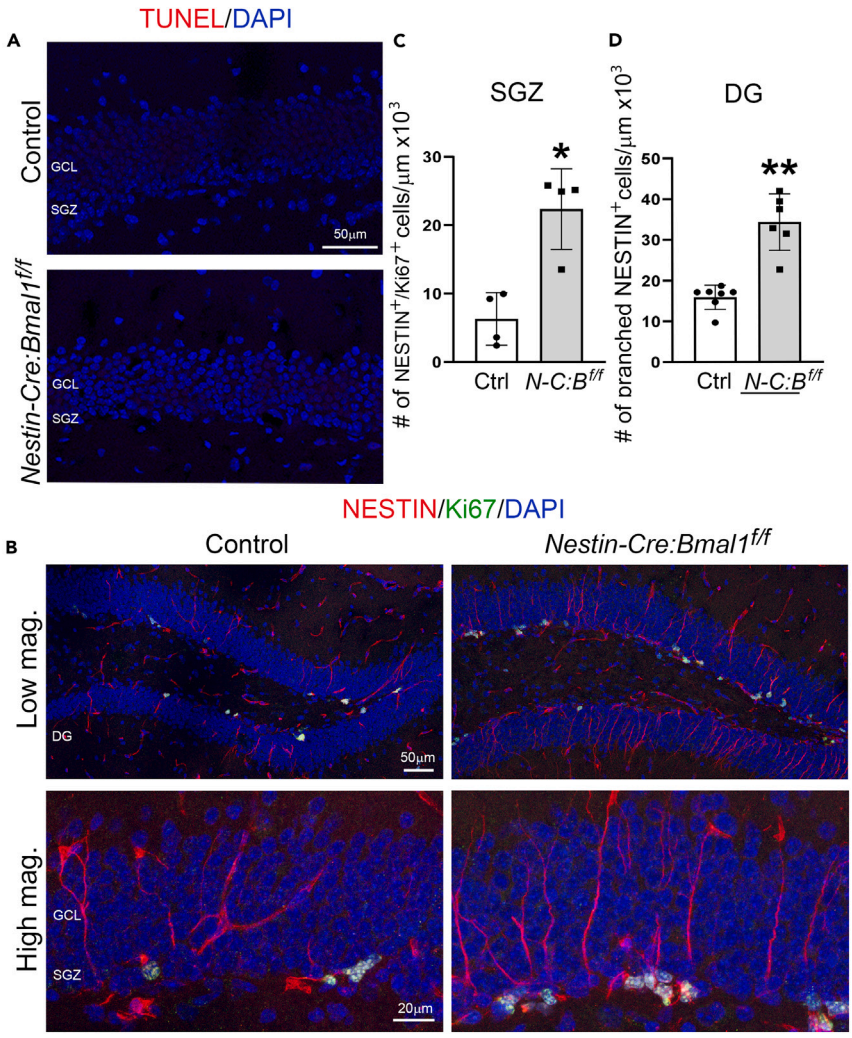

Figure 5. Reduced BMAL1 in SGZ cells induces cell proliferation and differentiation

(A) Confocal micrographs of the DG of control (Ctrl) and *Nestin-Cre:Bmal1*$^{f/f}$ (*N-C:B*$^{f/f}$) mice, stained with TUNEL (red). DAPI (blue) was used as a nuclear counterstain. Images from maximum intensity projections.

(B) Confocal images of the DG of control and *Nestin-Cre:Bmal1*$^{f/f}$ mice, stained with antibodies against NESTIN (red) and Ki67 (green). DAPI (blue) was used as a nuclear counterstain. Images from maximum intensity projections.

(C) The quantification of the SGZ in (B) (mean ± SD; a dot indicates one mouse brain; two-tailed t test).

(D) The quantification of the DG in (B) (mean ± SD; a dot indicates one hemisphere of the brain; two-tailed t test).

*p < 0.005; **p < 0.0001. See also Figure S5.

Reduced BMAL1 in SGZ cells induces cell proliferation and differentiation

We still cannot rule out any potential direct effects of NMDA on SGZ cells and BMAL1-independent mechanisms to alter SGZ states in excitotoxic DG lesions. To rule out this, we examined SGZ cell states in the DG composed of *Bmal1*-deleted GCs and SGZ cells. In this condition, no excitotoxic stimulus, NMDA, exists in the DG, but BMAL1 levels in GCs and SGZ cells are similar to excitotoxic DG lesions. We first confirmed reduced BMAL1 in the DG of *Nestin-Cre;Bmal1*$^{f/f}$ mice, of which the Cre-lox system deletes *Bmal1* in *Nestin*-expressing cells (Figure S5). Then, apoptosis was examined by TUNEL assays. Figure 5A shows no TUNEL signal in both control and *Nestin-Cre;Bmal1*$^{f/f}$ DGs, similar to Exito-1D and 3D in Figure 1E. Next, to examine SGZ cell proliferation, locations, and morphologies, coronal brain sections of control and *Nestin-Cre;Bmal1*$^{f/f}$ mice were stained with antibodies against NESTIN and Ki67, which are markers of SGZ cells and proliferating cells, respectively. Compared to the control, significantly increased numbers of total NESTIN$^+$ and Ki67$^+$/NESTIN$^+$ cells were detected in *Nestin-Cre;Bmal1*$^{f/f}$ mice, meaning increased proliferating SGZ cells (Figures 5B and 5C). We also compared the morphology of NESTIN$^+$ cells. More NESTIN$^+$ cells with either a radial process or neurite morphology were detected in *Nestin-Cre;Bmal1*$^{f/f}$ mice compared to the control (Figures 5B and 5D). This shows that reduced BMAL1 in SGZ cells and GCs is sufficient to increase proliferating and differentiating SGZ cells without other signals in excitotoxic DG lesions.

DISCUSSION

This study shows how hippocampal BMAL1 responds to a neurodegenerative condition, excitotoxicity, and its consequences. In the DG of the hippocampus, excitotoxicity damages GCs and reduces their BMAL1 levels. Neighbor adult neural stem cells and progenitors in the SGZ (SGZ cells) respond to damaged GCs and subsequently reduce their BMAL1 levels. Reduced SGZ-BMAL1 levels result in enhanced cell proliferation. Once SGZ cells differentiate into immature GCs, newly differentiating cells re-express BMAL1 to further differentiate into mature GCs, thereby replacing damaged GCs in the lesions. This study also shows that reduced BMAL1 in hippocampal neurons (GCs) and SGZ cells are involved in different cellular processes—affecting neighbor cells to change cell states and proliferation to increase cell numbers to replace damaged cells. Thus, this study provides perspectives on why understanding cell type-specific BMAL1 functions is important and why clock targeting (e.g., via BMAL1) must be specific to treat brain pathology rather than restoring all clocks as physiological rhythms with light therapy and melatonin administration.

This study focuses on the circadian transcription factor BMAL1. All brain cells contain circadian clocks to maintain homeostasis in various cellular and molecular processes, and BMAL1 is the key factor in operating these via thousands of clock gene expressions. Circadian clocks also monitor environmental changes to be synchronized. So, local circadian clocks may respond to microenvironmental changes in lesions and alter BMAL1 activities to effectively respond to them via its target gene expression changes. This can result in altered cellular and molecular homeostasis, which may work as signals for further processes like initiating repair systems or accelerating damage processes. Based on these, we hypothesized that microenvironmental changes in neurodegenerative conditions affect local BMAL1, and this information is conveyed to other cells using the synchronization mechanisms. This study shows that glutamate excitotoxicity affects neuronal and SGZ-BMAL1 directly or indirectly to initiate brain repair by SGZ-derived GCs. Since excitotoxicity does not affect BMAL1 levels in other cell types (e.g., astrocytes) in the lesions, the information SGZ-BMAL1 received is from damaged GC-BMAL1. In other words, neuronal BMAL1 changes can be specific signals to SGZ cells to inform a damaged cell type.

We confirmed that reduced BMAL1 in SGZ cells and GCs were sufficient to induce neurogenesis in the DG without other signals generated by excitotoxicity using *Nestin-Cre:Bmal1*$^{f/f}$ mice in Figure 5. Since *Bmal1* is genetically deleted in *Nestin*-expressing cells in this transgenic line, it can mimic reduced BMAL1 in GCs and SGZ cells. We chose this line to examine BMAL1 effects on neurogenesis in the DG without BMAL1-independent and NMDA-direct effects on SGZ cells. However, we need to consider that *Bmal1* is also deleted in *Nestin-Cre:Bmal1*$^{f/f}$ mouse glial cells. In other words, we cannot rule out some effects from *Bmal1* deleted glial cells, although Figures 2 and S3B hint that there may be no significant effects of glial BMAL1 on neurogenesis in excitotoxic DG lesions. Figures 2 and S3B show that BMAL1 levels were not changed in other cells (e.g., astrocytes, oligodendrocytes, and microglia) in the stratum radiatum, stratum lacunosum-moleculare, and molecular DG layer of excitotoxic hippocampal lesions. This means glial BMAL1 levels differ between the excitotoxicity model and *Nestin-Cre:Bmal1*$^{f/f}$ mice—no reduction and reduction, respectively. However, SGZ cell proliferation was induced in both conditions. This suggests that glial BMAL1 levels in excitotoxic hippocampal lesions do not significantly affect SGZ cell states.

Accumulated stem cell studies have found multiple factors (e.g., BDNF and NGF) that regulate NSC proliferation and differentiation.[39–41] However, many studies on NSCs were performed with *in vitro* systems and examined the effects of individual factors on neurogenesis. Recent studies about neuronal repairs focus on endogenous NSCs in the adult brain, which are enriched in the subventricular zone of the lateral ventricle and the SGZ of the hippocampus. Those studies found that hippocampal microenvironments set by exercise and activated hypothalamic neurons effectively promoted neurogenesis with improved cognition and memory in animal models of Alzheimer's disease.[42–44] This means communications between brain areas or cells—for example, between the hypothalamus, which includes the circadian pacemaker SCN, and the hippocampus—are necessary to improve brain functions. Activated hypothalamic neurons projecting to GCs in the DG improve recovery of hippocampal functions via neurogenesis by SGZ cells.[42,44] This suggests that enhanced communications between hippocampal neurons (GCs), SGZ cells, and other brain areas/cells are more effective for brain repairs than individual factor treatment on SGZ cells. Thus, further studies need to elucidate underlying molecular mechanisms and the cores organizing communications in various pathological conditions.

Limitations of the study

This study employed *Nestin-Cre:Bmal1*$^{f/f}$ mice to investigate the effects of reduced BMAL1 in GCs and SGZ cells in the DG. However, two limitations of this transgenic line have to be considered. One, *Bmal1* is genetically deleted from the embryonic stage in *Nestin-Cre:Bmal1*$^{f/f}$ mice. Although *Nestin-Cre:Bmal1*$^{f/f}$ mouse brain shows a normal structure, we still cannot rule out *Bmal1* deletion effects on brain development. We induced excitotoxicity in the adult mouse brain, meaning that *Bmal1*-expressing hippocampal neurons were exposed to excitotoxicity, resulting in reduced BMAL1. This suggests that there can be potential differences between genetically deleted *Bmal1* from the embryonic stage and insult-reduced BMAL1 in fully differentiated neurons. Two, *Bmal1* is deleted in the nervous systems of *Nestin-Cre:Bmal1*$^{f/f}$ mice—no specific *Bmal1* deletion in the DG of the hippocampus. Thus, we cannot rule out the potential effects of *Bmal1* deletion outside the DG on GCs and SGZ cells because the brain forms complex networks. Thus, further studies (1) in conditional *Bmal1* knockout mice, such as tamoxifen-induced stage-specific Cre-expressing mice, or (2) specific deletion of *Bmal1* in either GCs or SGZ cells in the DG of the adult brain by local infection of virus-expressing cell-type-specific Cre will help better understand the effects of reduced BMAL1 in excitotoxic DG lesions.

STAR★METHODS

Detailed methods are provided in the online version of this paper and include the following:

- KEY RESOURCES TABLE
- RESOURCE AVAILABILITY
  - Lead contact
  - Materials availability
  - Data and code availability
- EXPERIMENTAL MODEL AND STUDY PARTICIPANT DETAILS
  - Mice
  - Animal model of glutamate excitotoxicity
  - SGZ cell cultures
  - Mature neuronal cultures
- METHOD DETAILS
  - Immunostaining
  - Terminal deoxynucleotidyl transferase-mediated dUTP nick end labeling (TUNEL) assay
  - Imaging
  - RNA extraction and quantitative RT-PCR
- QUANTIFICATION AND STATISTICAL ANALYSIS

SUPPLEMENTAL INFORMATION

Supplemental information can be found online at https://doi.org/10.1016/j.isci.2024.108829.

ACKNOWLEDGMENTS

We thank Drs. Patrizia Casaccia and Ye He (CUNY Advanced Science Research Center), Charles J. Weitz (Harvard Medical School), and Liang Zhang (City University of Hong Kong) for helpful discussion. Dr. Geoffrey C. Y. Lau (City University of Hong Kong) for helpful discussion and technical support. Ms. Qingqing Lu (City University of Hong Kong) for technical support and graphic abstract. This study was supported by grants from the Research Grants Council of the Hong Kong Special Administrative Region, China (Project No. CityU 11103418, 11101019, and 11102220 to J.Y.K.) and Tung Biomedical Sciences Centre, City University of Hong Kong (Project No. CityU 9609310 to J.Y.K.).

AUTHOR CONTRIBUTIONS

X.Z. conducted the majority of the experiments in the manuscript. S.H. performed clock gene expression analysis in the hippocampus across a circadian cycle. X.Z. and J.Y.K. analyzed experimental data and designed the experimental plan. J.Y.K. supervised the project and wrote the manuscript.

DECLARATION OF INTERESTS

The authors declare no competing interests.

Received: July 12, 2023
Revised: October 11, 2023
Accepted: January 3, 2024
Published: January 9, 2024

REFERENCES

1. Panda, S., Antoch, M.P., Miller, B.H., Su, A.I., Schook, A.B., Straume, M., Schultz, P.G., Kay, S.A., Takahashi, J.S., and Hogenesch, J.B. (2002). Coordinated transcription of key pathways in the mouse by the circadian clock. Cell *109*, 307–320.
2. Acosta-Rodríguez, V.A., Rijo-Ferreira, F., Green, C.B., and Takahashi, J.S. (2021). Importance of circadian timing for aging and longevity. Nat. Commun. *12*, 2862.
3. Takahashi, J.S., Hong, H.K., Ko, C.H., and McDearmon, E.L. (2008). The genetics of mammalian circadian order and disorder: implications for physiology and disease. Nat. Rev. Genet. *9*, 764–775.
4. Gekakis, N., Staknis, D., Nguyen, H.B., Davis, F.C., Wilsbacher, L.D., King, D.P., Takahashi, J.S., and Weitz, C.J. (1998). Role of the CLOCK protein in the mammalian circadian mechanism. Science *280*, 1564–1569.
5. Takahashi, J.S. (2015). Molecular components of the circadian clock in mammals. Diabetes Obes. Metab. *17*, 6–11.
6. Lande-Diner, L., Boyault, C., Kim, J.Y., and Weitz, C.J. (2013). A positive feedback loop links circadian clock factor CLOCK-BMAL1 to the basic transcriptional machinery. Proc. Natl. Acad. Sci. USA *110*, 16021–16026.
7. Kim, J.Y., Kwak, P.B., and Weitz, C.J. (2014). Specificity in circadian clock feedback from targeted reconstitution of the NuRD corepressor. Mol. Cell *56*, 738–748.
8. Hirano, A., Fu, Y.H., and Ptáček, L.J. (2016). The intricate dance of post-translational modifications in the rhythm of life. Nat. Struct. Mol. Biol. *23*, 1053–1060.
9. Yamazaki, S., Numano, R., Abe, M., Hida, A., Takahashi, R., Ueda, M., Block, G.D., Sakaki, Y., Menaker, M., and Tei, H. (2000). Resetting central and peripheral circadian oscillators in transgenic rats. Science *288*, 682–685.
10. Meijer, J.H., Michel, S., Vanderleest, H.T., and Rohling, J.H.T. (2010). Daily and seasonal adaptation of the circadian clock requires plasticity of the SCN neuronal network. Eur. J. Neurosci. *32*, 2143–2151.
11. Morin, L.P., and Allen, C.N. (2006). The circadian visual system, 2005. Brain Res. Rev. *51*, 1–60.
12. Hannibal, J. (2002). Neurotransmitters of the retino-hypothalamic tract. Cell Tissue Res. *309*, 73–88.
13. Kahan, A., Mahe, K., Dutta, S., Kassraian, P., Wang, A., and Gradinaru, V. (2023). Immediate responses to ambient light in vivo

reveal distinct subpopulations of suprachiasmatic VIP neurons. iScience *26*, 107865.
14. Ding, J.M., Faiman, L.E., Hurst, W.J., Kuriashkina, L.R., and Gillette, M.U. (1997). Resetting the biological clock: mediation of nocturnal CREB phosphorylation via light, glutamate, and nitric oxide. J. Neurosci. *17*, 667–675.
15. Schurov, I.L., McNulty, S., Best, J.D., Sloper, P.J., and Hastings, M.H. (1999). Glutamatergic induction of CREB phosphorylation and Fos expression in primary cultures of the suprachiasmatic hypothalamus in vitro is mediated by co-ordinate activity of NMDA and non-NMDA receptors. J. Neuroendocrinol. *11*, 43–51.
16. Shigeyoshi, Y., Taguchi, K., Yamamoto, S., Takekida, S., Yan, L., Tei, H., Moriya, T., Shibata, S., Loros, J.J., Dunlap, J.C., and Okamura, H. (1997). Light-induced resetting of a mammalian circadian clock is associated with rapid induction of the mPer1 transcript. Cell *91*, 1043–1053.
17. Colwell, C.S. (2011). Linking neural activity and molecular oscillations in the SCN. Nat. Rev. Neurosci. *12*, 553–569.
18. Gachon, F., Nagoshi, E., Brown, S.A., Ripperger, J., and Schibler, U. (2004). The mammalian circadian timing system: from gene expression to physiology. Chromosoma *113*, 103–112.
19. Lu, Q., and Kim, J.Y. (2022). Mammalian circadian networks mediated by the suprachiasmatic nucleus. FEBS J. *289*, 6589–6604.
20. Micklem, C.N., and Locke, J.C.W. (2021). Cut the noise or couple up: Coordinating circadian and synthetic clocks. iScience *24*, 103051.
21. Chang, Y.C., and Kim, J.Y. (2020). Therapeutic implications of circadian clocks in neurodegenerative diseases. J. Neurosci. Res. *98*, 1095–1113.
22. Cedernaes, J., Osorio, R.S., Varga, A.W., Kam, K., Schiöth, H.B., and Benedict, C. (2017). Candidate mechanisms underlying the association between sleep-wake disruptions and Alzheimer's disease. Sleep Med. Rev. *31*, 102–111.
23. Leng, Y., Musiek, E.S., Hu, K., Cappuccio, F.P., and Yaffe, K. (2019). Association between circadian rhythms and neurodegenerative diseases. Lancet Neurol. *18*, 307–318.
24. Breen, D.P., Vuono, R., Nawarathna, U., Fisher, K., Shneerson, J.M., Reddy, A.B., and Barker, R.A. (2014). Sleep and circadian rhythm regulation in early Parkinson disease. JAMA Neurol. *71*, 589–595.
25. Dowling, G.A., Burr, R.L., Van Someren, E.J.W., Hubbard, E.M., Luxenberg, J.S., Mastick, J., and Cooper, B.A. (2008). Melatonin and bright-light treatment for rest-activity disruption in institutionalized patients with Alzheimer's disease. J. Am. Geriatr. Soc. *56*, 239–246.
26. Paus, S., Schmitz-Hübsch, T., Wüllner, U., Vogel, A., Klockgether, T., and Abele, M. (2007). Bright light therapy in Parkinson's disease: a pilot study. Mov. Disord. *22*, 1495–1498.
27. Rutten, S., Vriend, C., van den Heuvel, O.A., Smit, J.H., Berendse, H.W., and van der Werf, Y.D. (2012). Bright light therapy in Parkinson's disease: an overview of the background and evidence. Parkinsons Dis. *2012*, 767105.
28. Huang, S., Choi, M.H., Huang, H., Wang, X., Chang, Y.C., and Kim, J.Y. (2020). Demyelination Regulates the Circadian Transcription Factor BMAL1 to Signal Adult Neural Stem Cells to Initiate Oligodendrogenesis. Cell Rep. *33*, 108394.
29. Lananna, B.V., McKee, C.A., King, M.W., Del-Aguila, J.L., Dimitry, J.M., Farias, F.H.G., Nadarajah, C.J., Xiong, D.D., Guo, C., Cammack, A.J., et al. (2020). Chi3l1/YKL-40 is controlled by the astrocyte circadian clock and regulates neuroinflammation and Alzheimer's disease pathogenesis. Sci. Transl. Med. *12*, eaax3519.
30. Wang, X.L., Wolff, S.E.C., Korpel, N., Milanova, I., Sandu, C., Rensen, P.C.N., Kooijman, S., Cassel, J.C., Kalsbeek, A., Boutillier, A.L., and Yi, C.X. (2020). Deficiency of the Circadian Clock Gene Bmal1 Reduces Microglial Immunometabolism. Front. Immunol. *11*, 586399.
31. Dong, X.X., Wang, Y., and Qin, Z.H. (2009). Molecular mechanisms of excitotoxicity and their relevance to pathogenesis of neurodegenerative diseases. Acta Pharmacol. Sin. *30*, 379–387.
32. Dusart, I., Marty, S., and Peschanski, M. (1991). Glial changes following an excitotoxic lesion in the CNS–II. Astrocytes. Neuroscience *45*, 541–549.
33. Marty, S., Dusart, I., and Peschanski, M. (1991). Glial changes following an excitotoxic lesion in the CNS–I. Microglia/macrophages. Neuroscience *45*, 529–539.
34. Fuentealba, L.C., Obernier, K., and Alvarez-Buylla, A. (2012). Adult neural stem cells bridge their niche. Cell Stem Cell *10*, 698–708.
35. Breunig, J.J., Silbereis, J., Vaccarino, F.M., Sestan, N., and Rakic, P. (2007). Notch regulates cell fate and dendrite morphology of newborn neurons in the postnatal dentate gyrus. Proc. Natl. Acad. Sci. USA *104*, 20558–20563.
36. Lugert, S., Basak, O., Knuckles, P., Haussler, U., Fabel, K., Götz, M., Haas, C.A., Kempermann, G., Taylor, V., and Giachino, C. (2010). Quiescent and active hippocampal neural stem cells with distinct morphologies respond selectively to physiological and pathological stimuli and aging. Cell Stem Cell *6*, 445–456.
37. Zhao, C., Deng, W., and Gage, F.H. (2008). Mechanisms and functional implications of adult neurogenesis. Cell *132*, 645–660.
38. Tozuka, Y., Fukuda, S., Namba, T., Seki, T., and Hisatsune, T. (2005). GABAergic excitation promotes neuronal differentiation in adult hippocampal progenitor cells. Neuron *47*, 803–815.
39. Chen, J., Zacharek, A., Zhang, C., Jiang, H., Li, Y., Roberts, C., Lu, M., Kapke, A., and Chopp, M. (2005). Endothelial nitric oxide synthase regulates brain-derived neurotrophic factor expression and neurogenesis after stroke in mice. J. Neurosci. *25*, 2366–2375.
40. Cattaneo, E., and McKay, R. (1990). Proliferation and differentiation of neuronal stem cells regulated by nerve growth factor. Nature *347*, 762–765.
41. Han, J., Calvo, C.F., Kang, T.H., Baker, K.L., Park, J.H., Parras, C., Levittas, M., Birba, U., Pibouin-Fragner, L., Fragner, P., et al. (2015). Vascular endothelial growth factor receptor 3 controls neural stem cell activation in mice and humans. Cell Rep. *10*, 1158–1172.
42. Li, Y.D., Luo, Y.J., Xie, L., Tart, D.S., Sheehy, R.N., Zhang, L., Coleman, L.G., Jr., Chen, X., and Song, J. (2023). Activation of hypothalamic-enhanced adult-born neurons restores cognitive and affective function in Alzheimer's disease. Cell Stem Cell *30*, 415–432.e6.
43. Choi, S.H., Bylykbashi, E., Chatila, Z.K., Lee, S.W., Pulli, B., Clemenson, G.D., Kim, E., Rompala, A., Oram, M.K., Asselin, C., et al. (2018). Combined adult neurogenesis and BDNF mimic exercise effects on cognition in an Alzheimer's mouse model. Science *361*, eaan8821.
44. Li, Y.D., Luo, Y.J., Chen, Z.K., Quintanilla, L., Cherasse, Y., Zhang, L., Lazarus, M., Huang, Z.L., and Song, J. (2022). Hypothalamic modulation of adult hippocampal neurogenesis in mice confers activity-dependent regulation of memory and anxiety-like behavior. Nat. Neurosci. *25*, 630–645.
45. Schneider, C.A., Rasband, W.S., and Eliceiri, K.W. (2012). NIH Image to ImageJ: 25 years of image analysis. Nat. Methods *9*, 671–675.
46. Wu, G., Anafi, R.C., Hughes, M.E., Kornacker, K., and Hogenesch, J.B. (2016). MetaCycle: an integrated R package to evaluate periodicity in large scale data. Bioinformatics *32*, 3351–3353.
47. Kim, J.Y., Shen, S., Dietz, K., He, Y., Howell, O., Reynolds, R., and Casaccia, P. (2010). HDAC1 nuclear export induced by pathological conditions is essential for the onset of axonal damage. Nat. Neurosci. *13*, 180–189.

STAR★METHODS

KEY RESOURCES TABLE

REAGENT or RESOURCE	SOURCE	IDENTIFIER
Antibodies		
Mouse monoclonal anti βIII-tubulin	Sigma	Cat#T8578; RRID:AB_1841228
Rabbit polyclonal anti-BMAL1	Bethyl Laboratories	Cat#A302-616A; RRID:AB_10555918
Phospho-CREB (Ser133) (87G3) Rabbit mAb	Cell Signaling	Cat#14001; RRID:AB_2798359
Mouse monoclonal [Rat-401] to Nestin	abcam	Cat#ab6142; RRID:AB_305313
Ki-67 Monoclonal Antibody	Invitrogen	Cat#14-5698-80; RRID:AB_10853185
Mouse Anti-Cre Recombinase Monoclonal antibody	Millipore	Cat# MAB3120; RRID: AB_2085748
Alexa Fluor 594-donkey anti-rabbit	Jackson ImmnuoResearch	Cat#711-585-152; RRID:AB_2340621
Alexa Fluor 488-donkey anti-mouse	Jackson ImmnuoResearch	Cat# 715-545-150; RRID: AB_2340846
Alexa Fluor 594-donkey anti-mouse	Jackson ImmnuoResearch	Cat#715-585-150; RRID: AB_2340854
Alexa Fluor 488-donkey anti-rat	Jackson ImmnuoResearch	Cat#712-545-150; RRID:AB_2340683
Biological samples		
Mice brain samples	This paper	N/A
Chemicals		
N-methyl-D-aspartate (NMDA)	Sigma	Cat# M3262; CAS: 6384-92-5
TRIzol™ Reagent	Invitrogen	Cat#15596018
Critical commercial assays		
TUNEL BrightRed Apoptosis Detection kit	VAZYME	Cat# A113-02
Click-iT™ Plus TUNEL Assay	Invitrogen	Cat# C10617
PrimeScript RT reagent Kit with gDNA Eraser	Takara	Cat# RR047A
TB Green Premix Ex Taq (Tli RNase H Plus)	Takara	Cat# RR420
Experimental models: Organisms/strains		
Thy1-YFP mouse: B6.Cg-Tg(Thy1-YFP)16Jrs/J *Mus musculus*	The Jackson Laboratory	Cat# JAX:003709; RRID: IMSR_JAX:003709
Nestin-EGFP mouse: Tg(Nes-EGFP)33Enik/J *Mus musculus*	The Jackson Laboratory	Cat# JAX:033927; RRID:IMSR_JAX:033927
Nestin-cre mouse: B6.Cg-Tg(Nes-cre)1Kln/J *Mus musculus*	The Jackson Laboratory	Cat# JAX:003771; RRID:IMSR_JAX:003771
Gfap-cre mouse: B6.Cg-Tg(Gfap-cre) 77. 6Mvs/2J *Mus musculus*	The Jackson Laboratory	Cat# JAX:024098; RRID:IMSR_JAX:024098
Bmal1 floxed (*Bmal1*$^{f/f}$) mouse: (B6.129S4(Cg)-Arntl^{tm1Weit}/J *Mus musculus*	The Jackson Laboratory	Cat# JAX: 007668; RRID:IMSR_JAX:007668
Wild-type mouse: C57BL/6J *Mus musculus*	The Jackson Laboratory	Cat# JAX:000664; RRID:IMSR_JAX:000664
Oligonucleotides		
Primers for quantitative RT-PCR	This paper	STAR Methods
Software and algorithms		
ImageJ	Schneider et al.[45]	https://imagej.nih.gov/ij/
Prism 10	GraphPad	https://www.graphpad.com/
ZEN 3.2 lite	Carl Zeiss	https://www.zeiss.com/corporate/int/home.html

(*Continued on next page*)

Continued

REAGENT or RESOURCE	SOURCE	IDENTIFIER
NIS-Elements BR 5.21.00	Nikon	https://www.nikon.com
MetaCycle	Wu et al.[46]	https://github.com/gangwug/MetaCycle

RESOURCE AVAILABILITY

Lead contact

Further information and requests for resources and reagents should be directed to and will be fulfilled by the Lead Contact, Jin Young Kim (jinykim@cityu.edu.hk).

Materials availability

This paper does not generate new unique reagents.

Data and code availability

- All data reported in this paper will be shared by the lead contact upon request.
- This paper does not report original code.
- Any additional information required to reanalyze the data reported in this paper is available from the lead contact upon request.

EXPERIMENTAL MODEL AND STUDY PARTICIPANT DETAILS

Mice

Thy1-YFP (B6.Cg-Tg(Thy1-YFP)16Jrs/J; JAX stock# 003709), Nestin-EGFP (Tg(Nes-EGFP)33Enik/J; JAX stock# 033927), *Nestin-cre* (B6.Cg-Tg(Nes-cre)1Kln/J; JAX stock# 003771), *Bmal1 floxed* (*Bmal1*$^{f/f}$) mice (B6.129S4(Cg)-Arntl^{tm1Weit}/J; JAX stock# 007668 | Bmal1^{lox}), *Gfap-cre* (B6.Cg-Tg(Gfap-cre)77.6Mvs/2J; JAX stock# 024098), and C57BL/6J mice were used for this study. All mice were maintained in a 12:12 h light-dark (LD) cycle at 20°C–24°C with 50%–70% humidity. All mouse experiments were performed in accordance with the protocol approved by the Institutional Animal Research Ethics Sub-Committee of City University of Hong Kong and Department of Health, The Government of The Hong Kong Special Administrative Region. To delete *Bmal1* in neural cells or astrocytes, the Cre-lox system was used: *Nestin-cre* or *Gfap-cre* female was crossed with *Bmal1*$^{f/f}$ male. *Bmal1*$^{f/f}$ or wild-type mice were served as the control for the experiments performed with *Nestin-cre*:*Bmal1*$^{f/f}$ mice.

Animal model of glutamate excitotoxicity

N-methyl-D-aspartate (NMDA, 200 nL, 7.5 mg/mL; Sigma) in 1× phosphate buffer saline (PBS) was stereotaxically injected into the hippocampus of 8–14 week-old, either male or female mice at circadian time (CT)06 when the circadian transcription factor BMAL1 levels peak, and it starts transcription of its target genes. The injected coordinates related to bregma were used to reach the hippocampus, AP: −1.65, ML: ±1.05, DV: 1.7. After injection, mice were kept in a 12:12 h LD cycle for different periods: 2 days in LD followed by 1 day constant darkness (Excito-3D) or constant darkness 1 day (Excito-1D). Mouse brains were harvested at CT06 to perform further experiments.

SGZ cell cultures

The hippocampi from 8 to 12 weeks old C57BL/6J, either male or female mice, were dissected in Leibovitz's L-15 medium (GIBCO). The hippocampi were incubated in 0.1% (w/v) papain (Worthington) at 37°C for 30 min and mechanically dissociated by pipetting every 10 min. Then, dissociated SGZ cells were washed with Mouse Neural Stem Cell Expansion Medium (Millipore), followed by re-suspension in 2 mL of Mouse Neural Stem Cell Expansion Medium containing 20 ng/mL EGF and 2 mg/mL heparin (all from Millipore) and plated in a 24-well plate. During the culture period for 10 days (DIV 10) at 37°C with 5% CO_2, fresh culture media was changed every other day, and sphere-forming SGZ cells were harvested for further experiments. For inducing excitotoxicity, DIV 10 SGZ cells were treated with NMDA (50 μM; Sigma) for 24 h at 37°C with 5% CO_2. Corresponding vehicle (PBS) were treated as the control. Control and excitotoxicity-induced SGZ cells were subjected to quantitative RT-PCR.

Mature neuronal cultures

The cortices of embryonic day 17.5 C57BL/6J mice were dissected in Hanks' balanced salt solution (HBSS; Gibco). The cortices were trypsinized in 0.025% trypsin-EDTA at 37°C for 15 min and then neutralized in NM10 medium containing Dulbecco's Modified Eagle's Medium (DMEM) (Gibco), 10% fetal bovine serum (FBS) (Gibco), 20 mM HEPES (Gibco), and 1% Penicillin-Streptomycin (Sigma), at room temperature (RT) for 5 min. Then, tissues were mechanically triturated into dissociated cells in the neuronal culture media containing Neurobasal (Gibco) supplemented with B27 (Gibco), 10 mM GlutaMax (Gibco) and 1% Penicillin-Streptomycin (Sigma). Dissociated cells were plated on poly-D-lysine (MW 70,000–150,000; Sigma) coated tissue culture dishes. After 3-day culture at 37°C with 5% CO_2, primary cultures were treated with

5 μM of cytosine β-D-arabinofuranoside (Ara-C; Sigma) for 18 h to eliminate proliferating cells. Primary neurons were cultured for 10 more days at 37°C with 5% CO_2 to fully differentiate and then harvested for further experiments.

METHOD DETAILS

Immunostaining

Immunohistochemistry (IHC) was performed as described previously.[47] In brief, eyes were removed first, and mice were perfused with 4% (w/v) PFA in 1× PBS at CT06 and the brains were kept in 30% (w/v) sucrose. 20 μm coronal sections (−1.6 to −1.8 mm from bregma) were blocked in the blocking buffer: 10% (v/v) normal goat serum and 0.5% (v/v) Triton X-100 in PGBA buffer, containing (0.1% (v/v) gelatin, 1% (w/v) bovine serum albumin, 0.002% (w/v) sodium azide in 0.1M phosphate buffer (PB), for 30 min at RT. Then, sections were incubated with primary antibodies in the blocking buffer for overnight at 4°C. Next day, sections were washed with 0.1M PB three times and incubated with secondary antibodies (Jackson ImmunoResearch) in the blocking buffer for 1 h at RT. After washing with 0.1M PB three times, sections were mounted with mounting medium. For pCREB immunostaining, sections were incubated with Alexa Fluor 647 conjugated anti-pCREB antibodies in the blocking buffer for 3 h at RT. For NESTIN and Ki67 immunostaining, antigen retrieval was performed before blocking step. Briefly, brain sections were washed with 1× PBS and incubated in 10 mM citrate buffer for 10 min at 95°C. Nuclei were counterstained with 4′, 6-diamidino-2-phenylindole (DAPI, Vectashield) in the mounting medium. The following antibodies were used in this study: TUJ1 (T8578, Sigma), 1:1000; BMAL1 (A302-616A, Bethyl Laboratories), 1:1000; pCREB (14001, Cell Signaling), 1:200; NESTIN (ab6142, abcam), 1:100; Ki67 (14-5698-80, Invitrogen),1:500; Cre (MAB3120, Millipore), 1:1000; Alexa Fluor 594-donkey anti-rabbit, 1:400; Alexa Fluor 488-donkey anti-mouse, 1:400; Alexa Fluor 594-donkey anti-mouse, 1:400; Alexa Fluor 488-donkey anti-rat, 1:400 (all secondary antibodies from Jackson ImmunoResearch).

Terminal deoxynucleotidyl transferase-mediated dUTP nick end labeling (TUNEL) assay

TUNEL assay was performed using TUNEL BrightRed Apoptosis Detection kit (A113-02, VAZYME) or Click-iT Plus TUNEL Assay (C10617, Invitrogen). Briefly, for the TUNEL BrighRed Apoptosis Detection kit, coronal brain sections were immersed in 4% (w/v) PFA in 1× PBS for 30 min at RT, followed by washing with 1× PBS and incubated with 20 μg/mL Proteinase K solution (VAZYME) for 10 min at RT. Then, sections were washed with 1× PBS and incubated with 1× Equilibration Buffer (VAZYME) for 20 min at RT, followed by incubation in TdT incubation buffer (VAZYME) for 1 h at 37°C. After washing with 1× PBS, nuclei were counterstained with DAPI in the mounting medium (Vectashield). For Click-iT Plus TUNEL Assay, coronal sections were immersed in 4% (w/v) PFA in 1× PBS for 15 min at 37°C, followed by washing with 1 × PBS and incubated with 1 × Proteinase K solution (Invitrogen) for 15 min at RT. Then, sections were washed with 1 × PBS, followed by immersed in 4% (w/v) PFA in 1× PBS for 5 min at 37°C. After washing with 1 × PBS, sections were incubated in TdT Reaction Buffer (Invitrogen) for 10 min at 37°C, followed by incubation in TdT reaction mixture (Invitrogen) for 60 min at 37°C. Then, sections were washed with 3% BSA and 0.1% Triton X-100 in 1 × PBS for 5 min at RT, followed by incubation in Click-iT Plus TUNEL reaction cocktail (Invitrogen) for 30 min at 37°C. After washing with 3% BSA in PBS, nuclei were counterstained with DAPI in the mounting medium (Vectashield).

Imaging

Immuno-reactive cells were visualized using confocal microscopy (Carl Zeiss LSM 880 NLO with Airyscan Laser Confocal Microscopy System and Nikon A1R HD25 Confocal Microscope). At least 3-6 sections from one brain were imaged using a z stack, and 5 images from one section were acquired every 2 μm in the z-direction using Confocal Microscopes. Maximum intensity projections of images were created by NIS-Element Viewer 4.50 Nikon. To show the co-localization of pCREB and BMAL1, images at a single z-position were analyzed. All images were created and analyzed by either ZEN 3.2 lite or NIS-Elements BR 5.21.00 and quantified using ImageJ (NIH).

RNA extraction and quantitative RT-PCR

The hippocampi, cultured SGZ cells, and primary mature neurons were collected in TRIzol (Invitrogen). Total RNA was extracted following the manufacturer's instruction and cleaned using PrimeScript RT reagent Kit with gDNA Eraser (Takara). To obtain cDNA, 0.2–1 μg of total RNA was processed for reverse transcription (RT) using PrimeScript RT Master Mix (Takara). To compare mRNA levels, quantitative RT-PCR (qRT-PCR) was performed using SYBR Green PCR master mix (Takara) in Applied Biosystems QuantStudioTM 3 Real-Time PCR System. See table below for sequences of the primers used in this study. Ribosomal Proteins S13 (*Rps13*) and L30 (*Rpl30*) are used as control genes.

List of the primers used in this study

Gene	Forward sequence	Reverse sequence
Rps13	TCCCTCCCAGATAGGTGTAATCC	TCCTTTCTGTTCCTCTCAAGGT
Rpl30	GCTGGAGTCGATCAACTCTAGG	CCAATTTCGCTTTGCCTTGTC

(*Continued on next page*)

Continued

List of the primers used in this study

Gene	Forward sequence	Reverse sequence
Map2	CAGGTGGTGGACGTGTGAA AATTGAGAGTG	CACGCTGGACCTGCTTGGGGACTGTG
Thy1	AAGTCGGAACTCTTGGCACC	TCCAGGCGAAGGTTTTGGTT
Gfap	ACCAGCTTACGGCCAACAG	CCAGCGATTCAACCTTTCTCT
Itgam	ATGGACGCTGATGGCAATACC	TCCCCATTCACGTCTCCCA
Mbp	ACACGAGAACTACCCATTATGGC	CCAGCTAAATCTGCTGAGGGA
Bmal1	TGACCCTCATGGAAGGTTAGAA	GGACATTGCATTGCATGTTGG
Per1	CAGCTGGGCCGGTTTTG	CACTTTATGGCGACCCAACA
Per2	GCCTTCAGACTCATGATGACAGA	TTTGTGTGCGTCAGCTTTGG
Cry1	CTGGCGTGGAAGTCATCGT	CTGTCCGCCATTGAGTTCTATG
Nr1d2	TGAACGCAGGAGGTGTGATTG	GAGGACTGGAAGCTATTCTCAGA
cFos	TCCTTACGGACTCCCCAC	CTCCGTTTCTCTTCCTCTTCAG
Caspase3	TGTCATCTCGCTCTGGTACG	AAATGACCCCTTCATCACCA
Sox2	GCGGAGTGGAAACTTTTGTCC	GGGAAGCGTGTACTTATCCTTCT
Pdgfrα	ATGACAGCAGGCAGGGCTTCAACG	CGGCACAGGTCACCACGATCGTTT
P27	TCAAACGTGAGAGTGTCTAACG	CCGGGCCGAAGAGATTTCTG
Ki67	ACCATCATTGACCGCTCCTTT	AGGCCCTTGGCATACACAAA
NMDAR2A	CTACGCCAGGATTCTCTAAACCAG	CAGAAATGTCAGAATGGGCTACCT
NMDAR2B	AAGAAGAATCGGAACAAACTGCG	CCTTGTCTTTCAGGCTCACGCT

QUANTIFICATION AND STATISTICAL ANALYSIS

All data were presented as mean ± SD. All statistical analyses were performed using GraphPad Prism 10 (San Diego, CA). Student's *t* test (two-tails) was performed to calculate p-values. $p < 0.05$ was considered as statistically significant. Statistical analysis of circadian rhythms in Figure S2A was performed using an R package MetaCycle.